ENGINEERING RESEARCH JOURNAL (ERJ)
Vol. 51, No. 2 April. 2022, pp. 188-198
Journal Homepage: http://erj.bu.edu.eg

Effect of Friction Stir Processing Parameters on the Mechanical and Dynamic Responses of AA 5052-H32

Mohammed Gamil[a,*], W.M. Farouk[b] and Mamdouh I. Elamy[c,d]

[a]*Department of Mechanical Engineering, Faculty of Engineering at Shoubra, Benha University, Cairo, Egypt.*

[b]*Mechanical Engineering Department, Faculty of Engineering, Benha University, Benha, Egypt.*

[c]*Industrial Engineering Department, Faculty of Engineering, Northern Border University, Arar, Saudi Arabia.*

[d]*Production Engineering & Mechanical Design Department, Faculty of Engineering, Menoufia University, Menoufia, Egypt.*

[*]***Corresponding author:*** *mohammed.gamil@feng.bu.edu.eg*

Abstract: The present study investigates the friction stir processing (FSP) effect on the mechanical and dynamic response of AA5052-H32.FSP was applied on a 1.5 mm thick aluminium sheet at three rotational speeds (495 rpm, 850 rpm, 1660 rpm) and two longitudinal feed rates (24 mm/min, 42 mm/min). The processed samples were mechanically tested by tensile and micro-hardness tests. The macrostructure of the FSPed zone was also investigated. The highest detected ultimate tensile strength (207.5 MPa) was observed at 850 rpm and 42 mm/min. The FSPed conditions 1660 rpm and 24 mm/min provide the highest mean value of micro-hardness (66.57 HV) at lowest standard deviation (SD). The macrostructure showed the successful stirring process. The dynamic behavior was investigated at the processed conditions by applying free vibration analysis at different sets of boundary conditions. By introducing unified mechanical parameters, the mathematical finite element analysis (FEA) is efficient in computing the Eigen-nature of FSP. The experimental analysis was carried out using frequency response function (FRF) using hammering method. The comparison between experimental and numerical models showed the efficiency of the proposed mathematical model for the FSP. The change of rotational speed from 495 rpm to 850 rpm increases the fundamental natural frequency by 7.11%, while the change from 850 rpm to 1660 rpm decreases it by 13.1%. The change of boundary fixation from C-C to C-F decreases the fundamental natural frequency by an average of 40.22%.The highest damping factor was occurred at 1600 rpm, 42 mm/min, and C-F boundary fixation.

Keywords: Friction stir process; Aluminium alloys; Dynamic analysis; Finite element modeling; Frequency response function (FRF).

1. Introduction

Aluminium alloys offer good corrosion resistance, good ductility, high thermal conductivity, high toughness combined with good formability and good weld ability. In addition, Aluminium alloys have superior strength to weight ratio and high fracture toughness. Therefore, they are widely used as structural lightweight materials for many automobiles, aeronautics, railway vehicles, medical, chemical, and other industrial applications [1, 2]. FSP is a solid-state operation used to enhance the mechanical properties and to apply surface modifications. In addition, it is used for refining the microstructure. The tool rotation speed and longitudinal feed rate are the main parameters that

affect the mechanical behaviour [3, 4]. Initially, this method was almost used for magnesium and Al alloys, but as the technology progressed, it was used for other alloying systems, such as copper alloys, ferrous alloys, and bronze [5, 6].

Gamil et al. studied the effect of GNPs addition to AA 5052-H32 by the FSP on the thermo-mechanical properties. The strength was decreased meanwhile the hardness was increased in the FSPed zone [7]. In addition, the thermal conductivity was increased to great extent. Yu Chen et al. illustrated in their study that the tool pin eccentricity enhances material flow and refines grains at the FSPed zone of Al-5052 [8]. Moreover, Khodabakhshi et. al. distributed TiO_2 nanoparticles throughout AA 5052 to distribute the nanoparticles and to enhance the mechanical properties [9]. In another study he added GNPs to AA 5052-H32 and studied its effect on the microstructure [10]. Furthermore, Jeon et al. studied the graphene effect of on the mechanical behaviour of AA 5052-H32 [11].

The study of the dynamic behaviour has been conducted by many investigators [12-22]. For instance, Essam illustrated in his study the effect of the number of FSP passes on the dynamic and mechanical behaviour of AA 2024 [12]. Moreover, Huang et al. studied the effect of the FSP at different rotation speeds (from 500 to 1500 rpm) on the vibration fracture resistance and tensile properties of AA 5052. They found that the FSPed samples had not only better vibration fracture resistance but also better tensile properties [13]. The effect of rotational speeds and longitudinal feeds of the FSP on the dynamic behaviour of AA 5052-H32 is still under investigation and fewer reports are published in this regard.

The main target of the current paper is to study the effect of the FSP parameters (rotational speeds, longitudinal feed rates) on the mechanical and dynamic behaviour of AA 5052-H32. The mechanical analysis was studied in terms of tensile and micro-hardness tests. Moreover, the macrostructure was also investigated. In addition, the dynamic behaviour was applied at various boundary conditions, rotational speeds and longitudinal feed rates experimentally by FRF and by finite element analysis (FEA).

2. EXPERIMENTAL WORK

2.1. Materials and methods

Aluminium alloy AA 5052-H32 was used as strips of 150 mm length, 50 mm width and 1.5 mm thickness for the FSP. The chemical composition of the alloy is presented in Table 1. The tool geometry and the FSP parameters are illustrated in Table 2.

The FSP was applied at three different rotational speed (495, 850, 1660 rpm) and two different longitudinal feed rates (24, 42 mm/min). Figure 1a shows the setup used for fixing the work piece during the FSP, meanwhile Fig.1b shows a FSP sample with an extracted flat tensile test specimen according to ASTM E8M-04 with $25^{\pm 0.001}$ mm gauge length and $6^{\pm 0.001}$ mm width. The tensile tests were applied by using a computerized testing machine (walter + bai AG) at 0.5 mm/min strain rate. Moreover, small specimens (10 mm long) were cut for micro-hardness investigation. Vicker's hardness was measured (Innovatest Europe BV NEMESIS 9104) through the width of the FSPed zone at a step of 2.5 mm to cover all FSP zone (see Fig.1b)

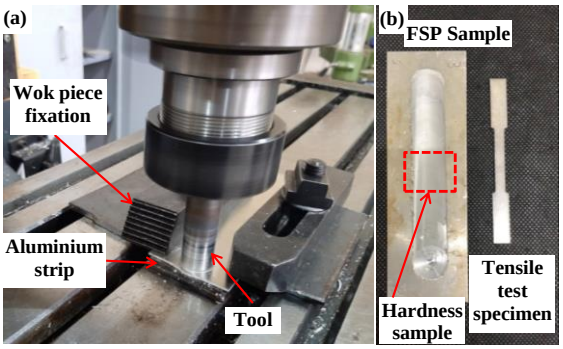

Fig 1. Real image for the (a) FSP of AA 5052-H32 by a vertical miller (b) FSP sample with a tensile test specimen extracted by wire cut.

Table 1. Chemical composition of AA 5052-H32 by wt%

Alloy	Alloying element (wt%)					
	Si	Fe	Cu	Mn	Mg	Al
AA 5052-H32	0.918	0.395	0.032	0.511	0.735	97.35

Table 2. FSP parameters and tool geometry

Sample number	Rotational speed (rpm)	Travel speed (mm/min)	Shoulder diameter (mm)	Pin diameter (mm)	Pin length (mm)	Shoulder type	Pin type
1	495	24	20	5	3	Concave	Threaded (right hand)
2	495	42					
3	850	24					
4	850	42					
5	1600	24					
6	1600	42					

2.2. Dynamic test setup by experiment dynamic test setup

A pulsed vibration test system shown in Fig. 2 is used for testing the FSPed samples. The test system has a pulse vibration measurement system, modal impact hammer (B & K 2302-5), laser vibrometer, and modal analysis software (fast Fourier transform analyzer B&K 3560) as shown in Fig. 2. A clamped-clamped (C-C), clamped-simply supported (C-S), simply supported (S-S) and clamped–free (C-F) boundaries fixations were used in the vibration tests. The FSPed test samples were excited by the help of the impact hummer. The vibration responses of the FSPed samples were recorded by the laser vibrometer. The fundamental natural frequencies and damping factors were obtained from the frequency response function (FRF). Every FRF was obtained by an average of three impact tests. The frequency response and coherence spectrum for the FSPed specimen with rotational speed 1600 rpm, longitudinal feed rate 24 mm/min and C-C boundary fixations are shown in Fig. 3.

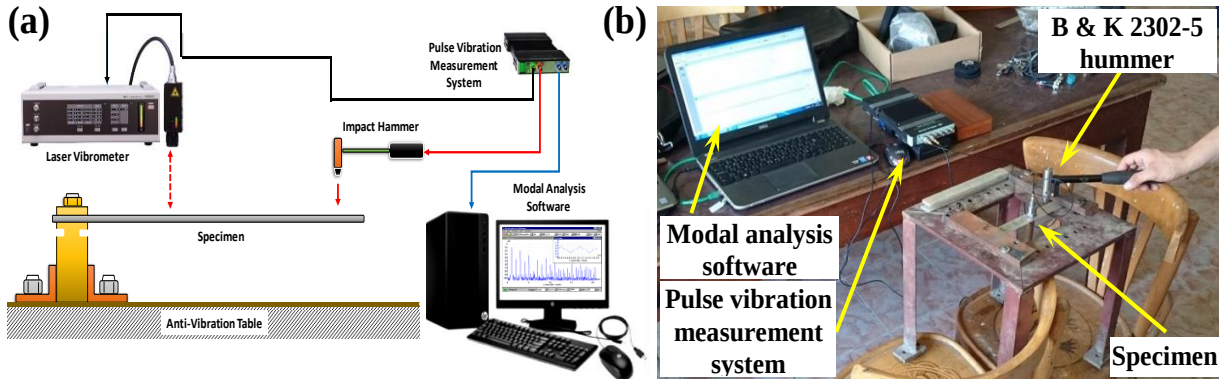

Fig 2. Pulsed vibration test system (a) Schematic diagram for C-F boundary fixation (b) Real image for C-C boundary fixation.

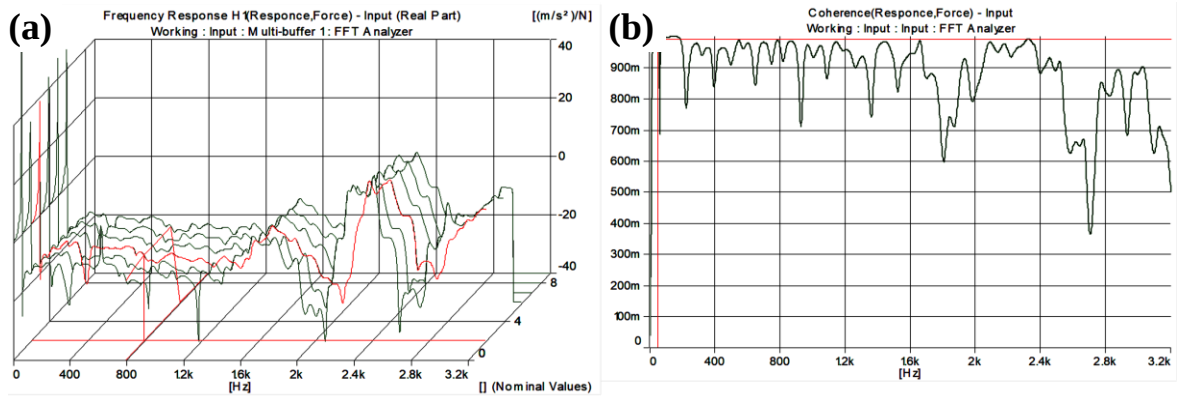

Fig 3. Spectrums of FSPed specimen with rotational speed 1600 rpm, longitudinal feed rate 24 mm/min and C-C boundary fixations (a) Frequency response spectrum (b) Coherence spectrum.

3. RESULTS AND DISCUSSION

3.1. Mechanical investigation

Figure 4 shows the tensile test results in terms of stress-strain curves for all the FSPed parameters. Figures 4 a,b show that the increasing of the feed rate from 24 mm/min to 42 mm/min results in an increase in the ultimate tensile strength (UTS).

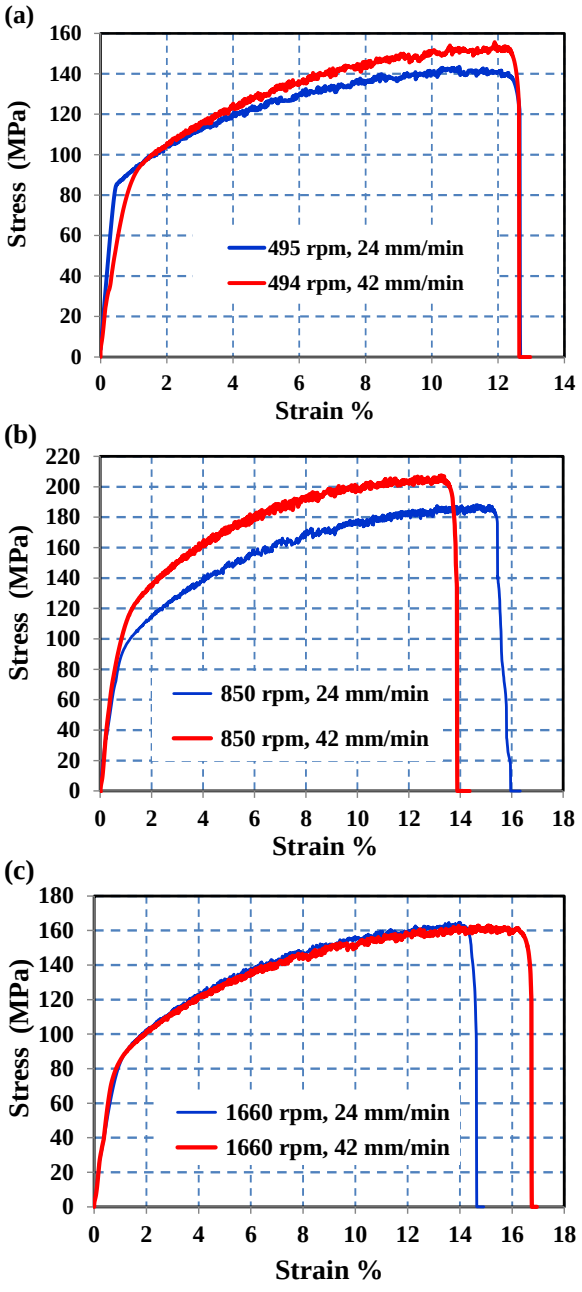

Fig 4. Tensile test results for the FSP of AA 5052-H32 (a) 495 rpm with 24 mm/min and 42 mm/min, (b) 850 rpm with 24 mm/min and 42 mm/min, (c) 1660 rpm with 24 mm/min and 42 mm/min.

On the other hand, there is no significant effect for the increasing of the feed rate at higher speed (1660 rpm) as illustrated in Figs. 4c. Figure 5 provides a clear comparison between the effect of the rotational speed and longitudinal feed rate on the UTS. Increasing the rotational speed from 495 rpm to 850 rpm; results in an increase in the UTS at the two applied feed rates. Further increase in the rotational speed to 1660 rpm lowered the UTS. So, the FSP for AA 5052-H32 will provides the highest UTS at 850 rpm and 42 mm/min (see Fig. 5).

Table 3 presents the Vickers micro-hardness results for the FSPed samples at 495 rpm, 850 rpm and 1660 rpm at a 24 mm/min feed rate (see Fig. 6). Eight testes were taken through the FSP zone each of 2.5 mm apart. The mean Vickers hardness for the FSP samples at the rotational speeds 495 rpm, 850 rpm and 1660 rpm at a 24 mm/min are 63.41 Hv, 61.22 Hv and 66.57 Hv respectively. There are no high variations between the measured hardness values through the FSP area especially at 1660 rpm (see Fig. 6).

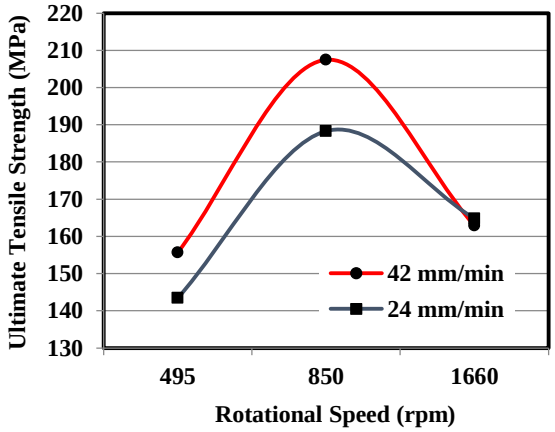

Fig 5. Effect of rotational speed and longitudinal feed rate of the FSP on the ultimate tensile strength.

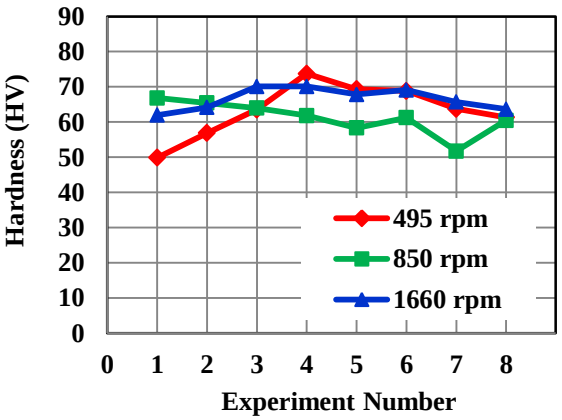

Fig 6. Micro-hardness results at 24 mm/min and different rotational speeds

Table 3. Vickers micro-hardness results for the FSPed samples at the three rotational speeds

Speed (rpm)	Vickers micro-hardness (HV)				
	Mean	Min	Max	SD	Range
495	63.41	49.86	73.74	7.58	23.88
850	61.22	51.74	66.83	4.72	15.09
1660	66.57	61.97	70.11	3.14	8.14

Figure 7 presents an optical macrograph for the cross sectional area of the FSP zone. The figure shows that the FSP is successfully applied and the aluminium alloy is already mechanically stirred by the effect of the too motion without the presence of any defects or cracks.

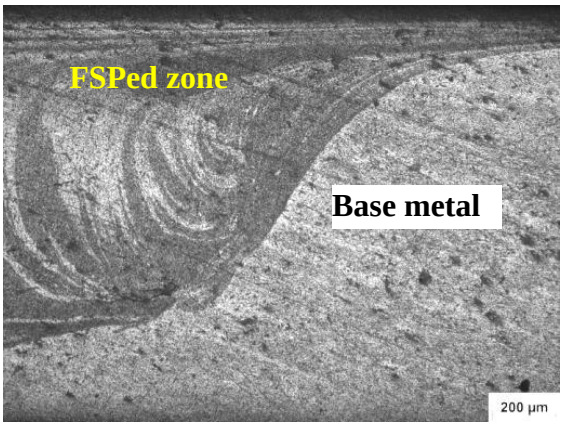

Fig 7. Optical macrographs for the cross-sectional area of the FSP zone for AA 5052-H32

3.2. Strain and kinetic energy for finite element modeling

The strain and kinetic energies are explained in equation (1) and equation (2) respectively.

$$V = \sum_{i=1}^{n} \frac{1}{2} \int_{\Omega i} \{\varepsilon\}_i^T \{\sigma\}_i d\Omega_i$$
$$= \sum_{i=1}^{n} \frac{1}{2} \int_{\Omega i} \{d\}^T [B]_i^T [D]_i [B]_i \{d\} d\Omega_i \quad (1)$$

$$T = \sum_{i=1}^{n} \frac{1}{2} \rho_i \int_{\Omega i} \{\dot{u}\}_i^T \{\dot{u}\}_i d\Omega_i$$
$$= \sum_{i=1}^{n} \frac{1}{2} \rho_i \int_{A} \int_{zi} \{\dot{d}\}_i^T \{\widehat{H}\}_i^T \{\widehat{H}\}_i \{\dot{d}\}_i d_{zi} dA \quad (2)$$

Where Ωi, A, $\{\dot{u}\}_i$ and ρirepresent are the volume, area, velocity field and mass density, respectively. {d} denotes the generalized displacement field, and $\{\widehat{H}\}_i$ is the through-thickness interpolation matrix of the common ith element. Furthermore, equation (2) can be rearranged in the following form

$$T = \sum_{i=1}^{n} \frac{1}{2} \int_{A} \{\dot{d}\}_i^T \{J\}_i d\Omega_i \{\dot{d}\}_i dA \quad (3)$$
$$\{J\}_i = \int_{zi} \rho_i \{\widehat{H}\}_i^T \{\widehat{H}\}_i dz_i \quad (4)$$

A set of shape functions should be determined to interpolate the geometry and variables within the finite element domain. To discretize the structure, we can choose an iso-parametric quadrangular finite element with four nodes [23]. Thus, that is

$$N_k(\xi, \eta) = \frac{1}{4}(1 + \xi_k \xi)(1 + \eta_k \eta), \quad k = 1, 2, 3, 4 \quad (5)$$

Consequently, it can be approximated to the elementary generalized displacement field, {de}, using the interpolation of the four nodal displacement fields, $\{d_k^e\}$. Specifically

$$\{d^e\}_{(2n+3)\times 1} = [N]_{(2n+3)\times(8n+12)} \{d_k^e\}_{(8n+12)\times 1} \quad (6)$$

where N is the shape functions matrix comprised by N_k. The benefits of this shape function include the reduced time-consuming property in comparison with other higher node shape functions. However, certain operations should be taken to prevent the shear lock from affecting the shape function.
Considering the strain energy and kinetic energy (i.e., Equations (1, 2)), and applying the extended Hamilton's principle, and the element mass matrix, $[M^e]$, the element stiffness matrix, $[K^e]$, can be obtained

$$[M^e] = \sum_{i=1}^{n} [M^e]_i = \sum_{i=1}^{n} \int_{A^e} [N]^T [J]_i [N] \, dA^e \quad (7)$$
$$[K^e] = \sum_{i=1}^{n} [K^e]_i = \sum_{i=1}^{n} \int_{A^e} [B]_i^T [D]_i [B]_i \, dA^e \quad (8)$$

where A^edenotes the area of the eth element.

To transform an element matrix from the local coordinate system into the global coordinate system prior to matrices assembly, a transformation matrix $[T_e]$ is applied for each element. Following that, using the node numbers of each element in the global coordinate system, n_E local-to-global connectivity matrices $[R^e]$ are created to assemble the n_E element matrices into a whole global matrix [24]. To be specific,

$$[M] = \sum_{e=1}^{n_E} [R^e]^T [T^e]^T [M^e][T^e][R^e] \quad (9)$$

$$[K] = \sum_{e=1}^{n_E} [R^e]^T [T^e]^T [K^e][T^e][R^e] \quad (10)$$

In the case of the free vibration problem, the global equations of motion can be expressed as follows:

$$[M]\{\ddot{q}_k\} + [M]\{q_k\} = \{0\} \quad (11)$$

In this case, $\{q_k\}$ represents the global degree of freedom.
In the free vibration problem, equation (11) leads to the following eigenvalue problem after we impose boundary conditions and restrictions on the directions of freedom in void regions [25].

$$|[K] - \gamma[M]|\{V\} = \{0\} \quad (12)$$

Where γ and $\{V\}$ is the eigenvalue and eigenvector respectively.
Finite element analysis (FEA) has been executed by using SOLID WORKS 2016 software. The fine mesh setting has been done in the FSPed zone. The FEM along with operating conditions for FSP are shown in Fig. 8. A typical aluminum beam of dimensions (150 × 20 × 1.5 mm) with various boundary conditions (C-C, C-S, S-S, C-F)and three types of rotational speeds and two types of longitudinal feed rates for the FSP of aluminum strip was modeled. The program computes the Eigen parameters using a code from the view point of equation 12 for the three types of rotational speeds and two types of longitudinal feed rates and the four boundary fixations as shown in Table 4.

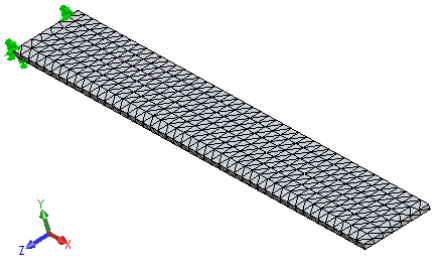

Fig 8. FEA of the FSP with C-F fixations.

Table 4. Fundamental natural frequencies at the four boundary conditions by FEA

No.	Feed (mm/min)	Speed (rpm)	Fundamental Natural Frequency (Hz)			
			C-C	C-S	S-S	C-F
0	Standard sample		367	273.4	108.6	65.6
1	24	495	330.2	247.6	89.1	56.8
2		850	358.5	265.3	96.8	59.4
3		1660	316.4	237.9	81.1	51.1
4	42	495	281.1	208.3	77	50.8
5		850	312.5	237.5	86.6	57.2
6		1660	261.4	190. 3	66.7	43.4

3.3. Dynamic Analysis of the FSP samples by FEA for dynamic behavior of AA 5052-H32 samples

The resonant frequencies and damping factors of the FSP of aluminum alloy AA 5052-H32 beam have been measured and analyzed at the different rotational speeds, longitudinal feed rates and boundary conditions. The measured and calculated values of the frequencies are tabulated in Table 5. Comparison between the experimental and finite element results of the frequencies indicates good agreement.

The FEA results are typically higher than the experimental ones, as given in Table 5, and this is because of the effects of air damping, clamping pressure, and dissipation of energy are not taken into consideration in the FEM.

Table 5 shows the experimental and finite element values of natural frequencies for different rotational speeds, feed rates, and boundary conditions. Furthermore, damping factors were also measured. It can be seen that the natural frequency of the test sample with rotational speed 850 rpm is relatively high compared with the others specimen. This is due to the maximum values of flexural elastic modules. It is also noticed that the maximum and minimum values of error between the finite element and experimentally measured natural frequencies of the C-C, C-S, S-S and C-F boundaries fixations are 1.79% and 0.85%, 1.98% and 0.69%, 4.95% and 0.99%, and 6.12% and 1.01% respectively.

Figure 9 (a,b) illustrates that the changing of the longitudinal feed rate from 24 mm/min to 42 mm/min results in a slight decrease in the natural frequencies by an average of 14.99%. The lower values of frequencies at 42 mm/min may be attributed to the low level of potential energy at this condition. It can be observed from Fig. 9 (a, b) that the test samples at a rotational speed of 1660 rpm have the lowest frequencies compared with the other test samples, while the test samples at the rotational speed of 850 rpm has the highest values this is due to the minimum and maximum values of flexural elastic modules and stiffness at these rotational speeds respectively.

The change of rotational speed from 495 rpm to 850 rpm increases the fundamental natural frequency by 7.11%, and the change of rotational speed from 850 rpm to 1660 rpm decreases the fundamental natural frequency by 13.1%.
From the view point of fixation, the rate of change of the eigen-frequencies are relatively high compared with the rate of change due to the rotational speed and longitudinal feed rate as shown in Fig. 9 and Table 5.

Table 5. Fundamental natural frequencies and damping ratios at the four boundary conditions (finite element and experimental)

No.	Feed (mm/min)	Speed (rpm)	Fundamental Natural Frequency (Hz) and damping ratio															
			C-C				C-S				S-S				C-F			
			ω_n			ξ	ω_n			ξ	ω_n			ξ	ω_n			ξ
			F.E	Ex	Error %	Ex	F.E	Ex	Error %	Ex	F.E	Ex	Error %	Ex	F.E	Ex	Error %	Ex
0	Standard sample		367	363.4	0.98	0.021	273.4	271.5	0.69	0.025	108.6	105.2	3.13	0.032	65.6	62.2	5.18	0.038
1	24	495	330.2	327.4	0.85	0.027	247.6	243.2	1.78	0.032	89.1	87.3	2.02	0.040	56.8	54.4	4.23	0.048
2		850	358.5	352.1	1.79	0.024	265.3	260.1	1.96	0.028	96.8	95.3	1.55	0.036	59.4	58.8	1.01	0.043
3		1660	316.4	313.2	1.01	0.033	237.9	233.2	1.98	0.039	81.1	80.3	0.99	0.049	51.1	49.6	2.94	0.059
4	42	495	281.1	278.4	0.96	0.037	208.3	205.2	1.49	0.044	77	73.9	4.03	0.055	50.8	48.3	4.92	0.066
5		850	312.5	309.5	0.96	0.035	237.5	234.3	1.35	0.041	86.6	84	3.00	0.052	57.2	53.7	6.12	0.062
6		1660	261.4	257.3	1.60	0.041	190.3	187.5	1.6	0.048	66.7	63.4	4.95	0.061	43.4	42.5	2.07	0.073

F.E: Finite element, Ex: Experimental, C-C: Clamped-Clamped, C-S: Clamped-Simply support, S-S: Simply support and C-F: Clamped –Free

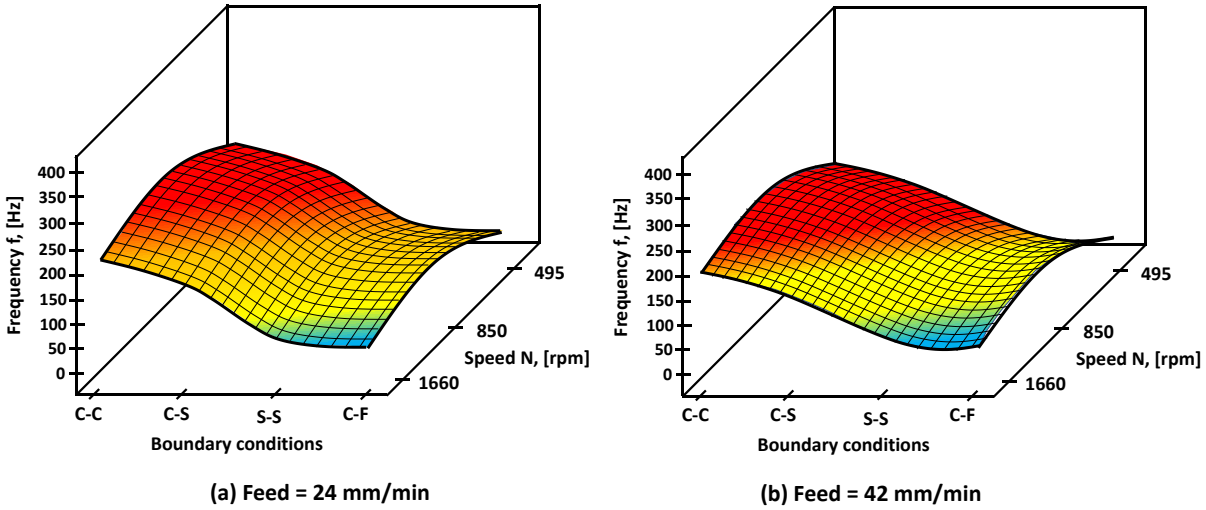

Fig 9. The relationship between the rotational speed, boundary conditions and natural frequency at feed rates of (a) 24 mm/min, (b) 42 mm/min.

It can be seen that the fixation C-C has a maximum natural frequency compared with the C-F which has the minimum value of natural frequency this is due to the maximum and minimum values of strain energies respectively.

The change of boundary fixation from C-C to C-F decreases the fundamental natural frequency by an average of 40.22%. This is due to the end fixation having a prominent influence in decreasing the frequencies. On the other hand, Table 5 and Fig. 10 (a, b) declares the effect of the rotational speed and boundary fixations on damping factor under the two applied longitudinal feed rates. It can be observed that the test samples with 24 mm/min longitudinal feed rate has lower damping factor if it is compared with the 42 mm/min test samples, this is due to the minimum and maximum values of dissipated energy.

Fig.10 (a, b) shows that the values of the damping factor are significantly varied with the state of rotational speed and boundary fixation in a reverse trend as compared with frequency (see Fig. 9). The high value of damping factor occurs at a rotational speed of 1600 rpm and C-F boundary fixation, this is may be attributed to the high level of dissipated energy at this condition. The damping factor in the test specimen with 1660 rpm is 1.3 times greater than those at 850 rpm and is 1.17 times greater than test specimen at 495 rpm. Changing the boundary fixation from C-C to C-F increases the damping factor by an average of 40.22% approximately.

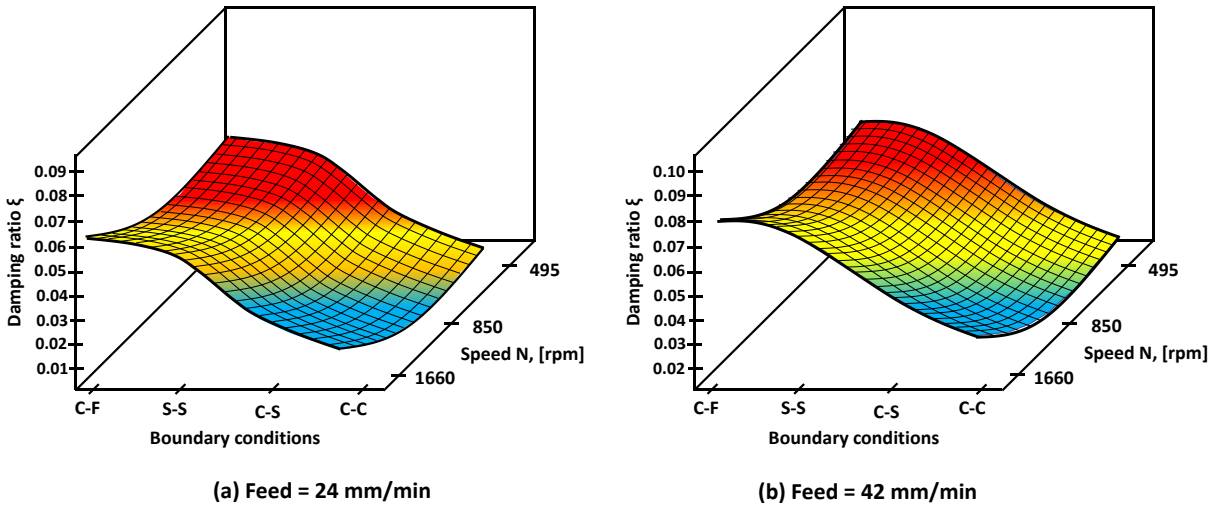

Fig 10. The relationship between damping factor, rotational speed, and boundary conditions at longitudinal feed rates of (a) 24 mm/min (b) 42 mm/min.

Figure 11 (a, b) show the comparison of the first five transverse mode shapes from FEA at the friction stir processing with a (C-F) and (C-C) fixations. It is seen that all corresponding mode shapes are similar.

It can be seen from the figures that the resultant amplitude plot for mode shape of the (C-C) fixation was not smooth like those of the mode shapes predicted by (C-F) fixation. This is because the dynamic response of friction stir processing beams depends on the force transducer locations in the system. Some complexity in the mode shapes can be attributed to the mass contribution of the force transducer to the overall system mass. Thus, the eigen-parameter may be controlled by changing the feed rate, rotational speed, and boundary fixations. Consequently, the obtained results provide a useful tool for the designer to select the proper rotational speed and boundary fixation to shift the natural frequencies as desired, particularly in the resonance zones of the FSP for AA 5052-H32.

3.4. Dynamic response of FSP

Matlab-based codes, version (8.1) was developed to analyze the dynamic response of the FSP for AA 5052-H32 beam under a harmonic peeling load based on the proposed theoretical investigations [26]. The analysis were performed for FSP for AA 5052-H32 beams of three types of rotational speed, two types of feed rate.

Figure 12 represent the frequency response of the FSP for the C-C boundary fixation of the specimen with the three applied rotational speeds and two longitudinal feed rates. It can be seen that the test specimens with 1660 rpm rotational speed have the highest amplitude. Meanwhile, the test samples with 850 rpm rotational speed have lower ones. The maximum amplitude was observed at a feed rate of 42 mm/min. It is higher than the measured amplitude at a feed rate 24 mm/min by almost 0.9%.

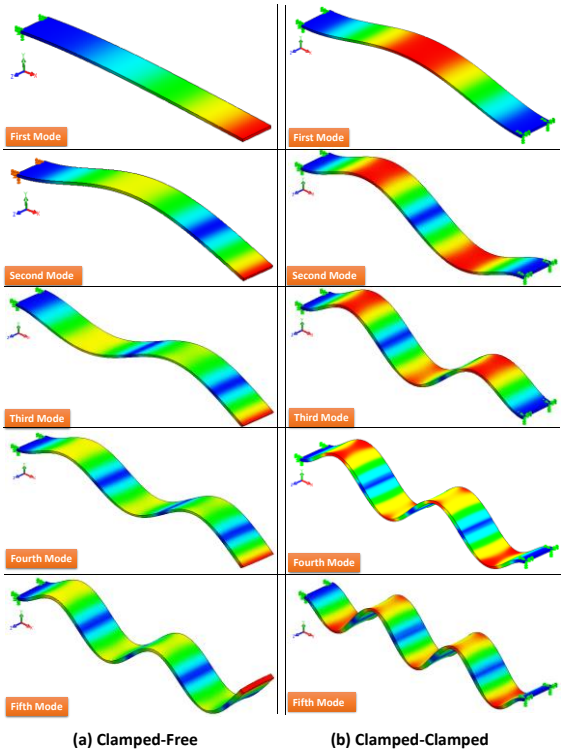

Fig 11. Comparison of the first five transverse mode shapes for clamped-free and fixations.

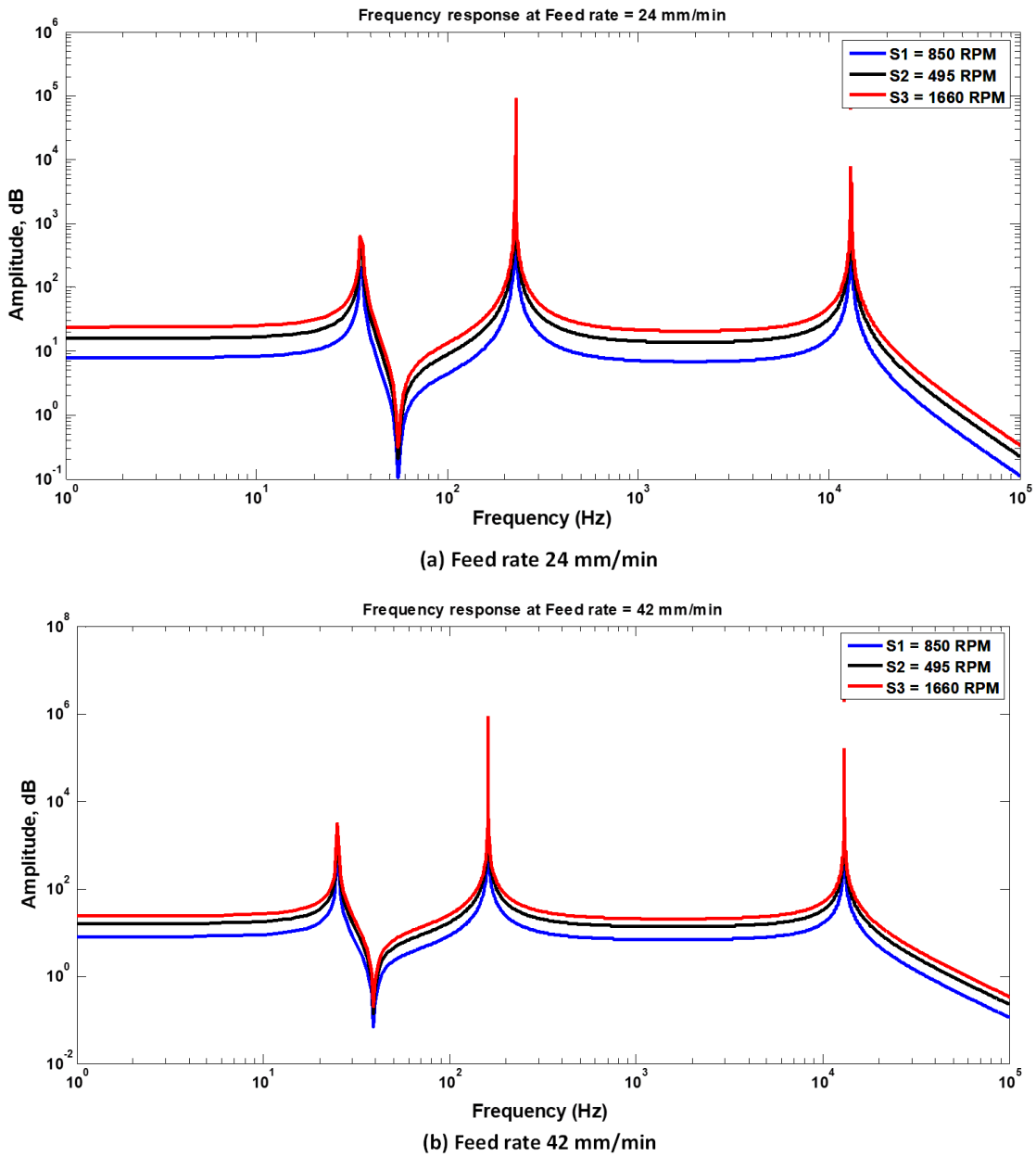

Fig 12. Theoretical model for the frequency response of the FSP at C-C boundary fixation at feed rates of (a) 24 mm/min, (b) 42 mm/min

4. Conclusions

- FSP was applied on a 1.5 mm sheet thickness of AA 5052-H32 at three different rotational speeds (495 rpm, 850 rpm, 1660 rpm) and two different longitudinal feed rates (24 mm/min, 42, mm/min).
- AA 5052-H32 is characterized for tensile and microhardness and the effect of the processing parameters on them were studied.
- The macrostructure of the FSPed cross-sectional was investigated to insure the quality of the FSP.
- The C.C and C.S boundary fixation are suitable for natural frequency in FSP of AA 5052-H32 where they give small error percentage, but in S.S and C.F boundary fixation they give a high value of error percentage.

- The theoretical model presented in this study, can obtain reasonable estimates of the resonance frequency and the damping ratio for FSP on AA 5052-H32 having different rotational speeds.

- The errors between F.E and Ex can be neglected because the almost of these values smaller than 5%.

- The values of errors increase with the change of the restraint of the structure from fixed to free.

5. ACKNOWLEDGEMENTS

The authors gratefully acknowledge Faculty of Engineering at (Shoubra, Benha), Benha University, Egypt. We also extend our thanks to the Industrial Engineering Department, Northern Border University, Arar, Saudi Arabia. Finally, we thank the Production Engineering & Mechanical Design Department, Menoufia University, Shebin El-Kom, Menoufia, Egypt

6. REFERENCES

[1] R. Rana, R. Purohit, and S. Das, "Reviews on the influences of alloying elements on the microstructure and mechanical properties of aluminum alloys and aluminum alloy composites," International Journal of Scientific and Research Publications 2, 2012, pp. 1-7.

[2] E. Georgantzia, M. Gkantou, and G. S. Kamaris, "Aluminium alloys as structural material: A review of research," Engineering Structures 227, 2021, p. 111372.

[3] R. S. Mishra and Z. Ma, "Friction stir welding and processing," Materials Science and Engineering: R: Reports 50, 2005, pp. 1-78.

[4] J.-T. Yoo, J.-H. Yoon, K.-J. Min, and H.-S. Lee, "Effect of friction stir welding process parameters on mechanical properties and macro structure of Al-Li alloy," Procedia Manufacturing 2, 2015, pp. 325-330.

[5] Z. Ma, "Friction stir processing technology: a review," Metallurgical and Materials Transactions A 39, 2008, pp. 642-658.

[6] A. P. Zykova, S. Y. Tarasov, A. V. Chumaevskiy, and E. A. Kolubaev, "A review of friction stir processing of structural metallic materials: Process, properties, and methods," Metals 10, 2020, p. 772.

[7] M. Gamil and M. M. Ahmed, "Investigating the thermo-mechanical properties of aluminum/graphene nano-platelets composites developed by friction stir processing," International journal of precision engineering and manufacturing 21, 2020, pp. 1539-1546.

[8] Y. Chen, H. Wang, X. Wang, H. Ding, J. Zhao, F. Zhang, and Z. Ren, "Influence of tool pin eccentricity on microstructural evolution and mechanical properties of friction stir processed Al-5052 alloy," Materials Science and Engineering: A 739, 2019, pp. 272-276.

[9] F. Khodabakhshi, A. Simchi, A. Kokabi, M. Sadeghahmadi, and A. Gerlich, "Reactive friction stir processing of AA 5052–TiO2 nanocomposite: process–microstructure–mechanical characteristics," Materials Science and Technology 31, 2015, pp. 426-435.

[10] F. Khodabakhshi, M. Nosko, and A. P. Gerlich, "Effects of graphene nano-platelets (GNPs) on the microstructural characteristics and textural development of an Al-Mg alloy during friction-stir processing," Surface and Coatings Technology 335, 2018, pp. 288-305.

[11] C.-H. Jeon, Y.-H. Jeong, J.-J. Seo, H. N. Tien, S.-T. Hong, Y.-J. Yum, S.-H. Hur, and K.-J. Lee, "Material properties of graphene/aluminum metal matrix composites fabricated by friction stir processing," International Journal of Precision Engineering and Manufacturing 15, 2014, pp. 1235-1239.

[12] E. B. Moustafa, "Dynamic characteristics study for surface composite of AMMNCs matrix fabricated by friction stir process," Materials 11, 2018, p. 1240.

[13] K.-T. Huang, T.-S. Lui, and L.-H. Chen, "Effect of dynamically recrystallized grain size on the tensile properties and vibration fracture resistance of friction stirred 5052 alloy," Materials Transactions 47, 2006, pp. 2405-2412.

[14] K.-T. Huang, T.-S. Lui, and L.-H. Chen, "Pre-treated effect of friction stir processing of Al Alloy 5052 on vibration fracture behavior under resonant vibration," Materials Transactions 46, 2005, pp. 3051-3058.

[15] N. Srikanth, K. K. Tun, and M. Gupta, "Finite element based energy dissipation studies of Al-SiC composites," Journal of Composite Materials 37, 2003, pp. 1385-1410.

[16] I. Yesilyurt and H. Gursoy, "Estimation of elastic and modal parameters in composites using vibration analysis," Journal of Vibration and Control 21, 2015, pp. 509-524.

[17] N. Yuvaraj and S. Aravindan, "Fabrication of Al 5083/B4C surface composite by friction stir processing and its tribological characterization," Journal of Materials Research and Technology 4, 2015, pp. 398-410.

[18] E. Moustafa, "Effect of multi-pass friction stir processing on mechanical properties for AA2024/Al_2O_3 nanocomposites," Materials 10, 2017, p. 1053.
[19] K. Venkateswara Reddy, R. Bheekya Naik, S. Yadav, G. Madhusudhan Reddy, and R. Arockia Kumar, "Measurement of Elastic Modulus and Damping Properties of Friction Stir Processed Pure Metals Using Impulse Excitation Technique," in Advances in Applied Mechanical Engineering, ed: Springer, 2020, pp. 521-528.
[20] N. A. Nazri, M. S. M. Sani, M. N. Mansor, and S. N. Zahari, "Model Updating of Friction Stir Welding for Aluminium and Magnesium Plate Structure," in MATEC Web of Conferences, 2018, p. 04004.
[21] K. V. Reddy, R. B. Naik, G. M. Reddy, and R. A. Kumar, "Damping capacity of friction stir processed commercial pure aluminium metal," Materials Today: Proceedings 27, 2020, pp. 2061-2065.
[22] S. N. Zahari, M. S. M. Sani, N. A. Husain, M. Ishak, and I. Zaman, "Dynamic analysis of friction stir welding joints in dissimilar material plate structure," Jurnal Teknologi 78, 2016.
[23] S. Hügül, "Vibration analysis of systems subjected to moving loads by using the finite element method," Fen Bilimleri Enstitüsü, 2005.
[24] S. S. Rao, "The finite element method in engineering (Quinta)," ed: Oxford: Elsevier/Butterworth Heinemann, 2011.
[25] O. C. Zienkiewicz, R. L. Taylor, and J. Z. Zhu, The finite element method: its basis and fundamentals: Elsevier, 2005.
[26] M. R. HATCH, "MATLAB ANSYS and," ed: Chapman & Hall/CRC, 2001.